

# On the inner–outer core density contrast from PKiKP/PcP amplitude ratios and uncertainties caused by seismic noise

Hrvoje Tkalčić,<sup>1</sup> Brian L. N. Kennett<sup>1</sup> and Vernon F. Cormier<sup>2</sup>

<sup>1</sup>Research School of Earth Sciences, The Australian National University, Mills Road, Jaeger Building 61, Canberra, ACT 0200, Australia.

E-mail: Hrvoje.Tkalcic@anu.edu.au

<sup>2</sup>Department of Physics, University of Connecticut, 2152 Hillside Road U-3046, Storrs, CT 06269-3046, USA

Accepted 2009 June 11. Received 2009 June 11; in original form 2008 December 9

## SUMMARY

The inner core boundary (ICB) of the earth is characterized by a discontinuous change in elastic properties between the liquid outer and solid inner core. In the ray theory approximation, a measure of the density contrast at the ICB is given by the amplitude ratio of *P* waves reflected from the core–mantle boundary (CMB; PcP waves) and the ICB (PKiKP waves), since that ratio conveniently appears in an explicit form in the transmission/reflection coefficient equations. The results for inner–outer core density contrast derived from direct amplitude picks of these waves in the time domain have varied significantly among different authors.

The transmission/reflection coefficients on the liquid–solid and solid–liquid boundaries derived from ground displacements enable a direct comparison between the amplitude measurements on displacement seismograms in the time domain and theoretical values. A new approach is proposed and applied to integrate effects of microseismic and signal-generated noise with the amplitude measurements, thus providing a direct maximal uncertainty measure. To suppress the effects of varying radiation pattern and distinctively different ray paths at longer epicentral distances, this new method was applied to high-quality arrivals of PcP and PKiKP waves from a nuclear explosion observed at epicentral distances 10°–20° from recording stations. The resulting uncertainties are high precluding precise estimates of the ICB density contrast, but provide a robust estimate of an upper bound from body waves of about 1100 kg m<sup>−3</sup>. Median values of two amplitude ratios observed around 17° epicentral distance indicate a small density contrast of 200–300 kg m<sup>−3</sup> and suggest the existence of zones of suppressed density contrast between the inner and the outer core, a density contrast stronger than 5000 kg m<sup>−3</sup> at the CMB, or a combination of both.

**Key words:** Time-series analysis; Composition of the core; Body waves; Wave propagation.

## 1 INTRODUCTION AND MOTIVATION

The size and nature of the major discontinuities in Earth can be related to the age of the inner core and the energy needed to sustain Earth's magnetic field. The density discontinuity  $\Delta\rho$  at the inner core boundary (ICB) and the radius of the inner core are invaluable constraints for calculations of thermal evolution of the Earth's core (e.g. Stevenson *et al.* 1983; Buffett *et al.* 1996; Nimmo *et al.* 2004). The gradual cooling of the outer core causes the inner core to solidify and the ICB to advance. The region of mixed solid and liquid in which the phase change is actively occurring is much smaller than the typical wavelength of body waves, making it indistinguishable from a first-order discontinuity in density and elastic moduli (Loper 1983).

Early seismological estimates of  $\Delta\rho$  at the ICB from the amplitude ratio of PKiKP/PcP (Bolt & Qamar 1970; Souriau & Souriau 1989) were generally sparse in global coverage of the ICB and predicted a  $\Delta\rho$  higher by factors of 2 or more than the 550–600 kg m<sup>−3</sup> density contrast predicted from normal modes (Dziewonski & Anderson 1981). Shearer & Masters (1990) considered both body waves and normal modes, but found only two probable appearances of PcP and PKiKP waves on the same seismogram. From body waves, they concluded that  $\Delta\rho$  at the ICB must be less than 1000 kg m<sup>−3</sup> while normal modes required even lower values (550 kg m<sup>−3</sup>). Masters & Gubbins (2003) recalculated the density jump from normal mode data showing that the previous mode estimate was too low and could be raised to 820 kg m<sup>−3</sup>. Both that study and a recent study by Gubbins *et al.* (2008), however, emphasize that the spread in depth of the mode resolution kernels for density makes it difficult to discriminate a higher density jump localized at the ICB from the integrated effect of a density gradient above the ICB followed by a smaller  $\Delta\rho$  at the ICB. The preferred model of Gubbins *et al.* (2008), compatible with core thermal history

calculations, has  $\Delta\rho$  of  $600 \text{ kg m}^{-3}$  at the ICB with a reduced  $P$ -velocity gradient and increased density gradient in the lowermost outer core. These gradients are consistent with a compositional gradient above the solidifying inner core. Song & Helmberger (1995) and Zou *et al.* (2008) found evidence of a reduced  $P$ -velocity gradient from the traveltimes of PKP waves diffracted around the ICB, and this feature is present in global models of seismic velocity that are constrained by carefully analysed traveltimes of multibranch PKP waves (Kennett *et al.* 1995). Recent investigations by Koper & Pyle (2004) and Koper & Dombrovskaya (2005) using beams constructed from short-period array observations of P, PcP and PKiKP favor a small value of  $\Delta\rho$  of  $520 \pm 240 \text{ kg m}^{-3}$ , more consistent with original estimates from normal modes.

As observations of PKiKP have increased in the distance range where it is a weak, partially reflected wave, there have been increased suggestions that variability in its amplitude may be due to true lateral variability in the physical properties in the region of the ICB, including variability in the  $P$  velocity,  $S$  velocity and density contrasts, possible variability in ICB topography, and variability in volumetric scattering and attenuation on either side of the ICB. Koper & Dombrovskaya (2005) suggested that evidence of this lateral variation in ICB properties is regional coherence in the PKiKP/P ratio that varies by up to two orders of magnitude. Modifying the idea of beam forming signals from observations at arrays of receivers, Krasnoshchekov *et al.* (2005) measured absolute PKiKP amplitudes from waveforms stacked from arrays of different nuclear explosions at known locations around major test sites. To form beams they normalized the strength of each source to a fixed explosive yield. They found that observed amplitudes near  $50^\circ$ – $100^\circ$  could not be fit with standard earth models of the ICB region and suggested that the variability of the inferred ICB density contrast ( $450$ – $1660 \text{ kg m}^{-3}$ ) may simply signify a mosaic of lateral variation in the physical properties across the ICB. Their interpretations included the possibility of strong gradients in shear modulus on either the outer or inner core side of the ICB. Possibly consistent with observed lateral variations in  $P$ -velocity gradient in the lowermost outer core (Yu *et al.* 2005) is a region of laterally varying viscosity associated with a frequency dependent shear modulus in the lowermost outer core (Cormier 2009). Lateral variations in this region above the ICB may be coupled to lateral variation in the solidification process of the inner core (Cormier 2007) and lateral variations of flow in the outer core (Aubert *et al.* 2008).

Variation in the amplitude ratio PKiKP/PcP ratio used to infer  $\Delta\rho$  will include the propagation effects of lateral variations concentrated near the core–mantle boundary (CMB), possibly the ICB region, and the crust and upper mantle. We examine the effects of lateral variation near the CMB and the crust and upper mantle in a separate paper (Tkalčić *et al.* 2009). Our aim in this paper is to first estimate the effects on variability of the PKiKP/PcP ratio that are solely due to ambient and signal-generated (scattered) noise. When the effects of noise and shallower structure are understood, it may then be possible to better estimate the true lateral variation that may be concentrated in the ICB region.

Keeping in mind all the limitations imposed by a number of assumptions made about Earth and the ray theory used, it is attempted here to reduce the severity of the effects of ambient and signal-generated noise and provide a robust estimate of uncertainties in the PKiKP/PcP amplitude ratio measurements. This is accomplished in two steps.

(1) High quality arrivals of PKiKP and PcP waves on the same seismogram were identified on displacement seismograms for a nuclear explosion event at a short epicentral distance. This alleviates both the uncertainties associated with the radiation pattern and unequal sampling of the mantle due to different ray paths, and helps to avoid problems of comparing measurements from different events.

(2) A method that combines amplitude measurements with seismic noise and allows consequent maximum uncertainty estimates was designed and applied to new observations of PKiKP and PcP waves on the same seismogram.

## 2 TRANSMISSION/REFLECTION COEFFICIENTS FOR THE INNER CORE AND CORE–MANTLE BOUNDARIES AS A FUNCTION OF THE ANGLE OF INCIDENCE AND THE EPICENTRAL DISTANCE

Expressions for the transmission/reflection coefficients of elastic waves for a pair of homogeneous half-spaces in contact are well known and available in many seismology texts. Care, however, must be exercised in copying typeset equations, which tend to accumulate errors in proportion to the number of steps leading to their publication. The safest procedure for calculation is excise the coefficient subroutines of well-tested and commented computer codes for synthesizing seismograms, for example, the coefficient routines associated with the codes described in Seismological Algorithms (Doornbos 1988). For the results shown in this paper, we rederived expressions for reflection/transmission coefficients at solid–liquid and liquid–solid boundaries from ground displacements using the same set-up and mnemonics as in Bolt & Qamar (1970), but checked our results against those calculated by routines distributed with Seismological Algorithms. Our computed amplitude ratios for PKiKP/PcP in Section 3 include the effects of reflection and transmission through all first-order discontinuities in specific earth models as well the effects of geometric spreading. These results agreed with the amplitude ratios predicted from the product of factors occurring in the expressions for ray theoretical amplitude computed from dynamic ray tracing routines (e.g. Červený 2001).

A system of three equations with three unknowns obtained for the liquid–solid boundary is

$$\begin{bmatrix} \beta_2 (\tan^2 \varphi^{\text{iii}} - 1) & 0 & 2\alpha_2 \tan \varphi^{\text{ii}} \\ \beta_2 & -\alpha_1 \tan \varphi & -\alpha_2 \tan \varphi^{\text{ii}} \\ 2\frac{\beta_2^3}{\alpha_1^2} \tan \varphi^{\text{iii}} & \frac{\rho_1}{\rho_2} \alpha_1 \sec^2 \varphi & -\alpha_2 \frac{\beta_2^2}{\alpha_1^2} (\tan^2 \varphi^{\text{iii}} - 1) \end{bmatrix} \begin{bmatrix} B/A \\ C/A \\ D/A \end{bmatrix} = \begin{bmatrix} 0 \\ -\alpha_1 \tan \varphi \\ -\frac{\rho_1}{\rho_2} \alpha_1 \sec^2 \varphi \end{bmatrix}. \quad (1)$$

In eq. (1), a  $P$  wave with amplitude  $A$  of ground motion is incident onto the horizontal liquid–solid boundary at an angle  $\varphi$ .  $C$  is the amplitude of the reflected  $P$  wave (at an angle  $\varphi^i$ ) and  $D$  is the amplitude of the transmitted  $P$  wave (at an angle  $\varphi^{ii}$ ).  $B$  is the amplitude of the refracted SV wave (at an angle  $\varphi^{iii}$ ). The angles are measured from the horizontal, as in Bolt & Qamar (1970).  $\alpha_1$  and  $\rho_1$  are the compressional velocity and density of the liquid, while  $\alpha_2$ ,  $\beta_2$  and  $\rho_2$  are the compressional and shear velocities and density of the solid. The  $x$ -axis is positive eastwards and  $z$ -axis is positive upwards. Note that the direction of SV motion is rotated for  $90^\circ$  from  $P$  motion using the right-hand coordinate system convention. Three boundary conditions that are considered for the liquid–solid boundary are: (1) normal displacements are continuous, (2) tangential stresses vanish and (3) normal stresses are continuous.

A similar system of equations obtained for the solid–liquid boundary is

$$\begin{bmatrix} \beta_2 (1 - \tan^2 \varphi^{iii}) & 2\alpha_2 \tan \varphi & 0 \\ \beta_2 & \alpha_2 \tan \varphi & \alpha_1 \tan \varphi^i \\ 2 \frac{\beta_2^3}{\alpha_1^2} \tan \varphi^{iii} & \alpha_2 \frac{\beta_2^3}{\alpha_1^2} (\tan^2 \varphi^{iii} - 1) & -\frac{\rho_1}{\rho_2} \alpha_1 \sec^2 \varphi^i \end{bmatrix} \begin{bmatrix} B/A \\ C/A \\ D/A \end{bmatrix} = \begin{bmatrix} 2\alpha_2 \tan \varphi \\ \alpha_2 \tan \varphi \\ -\alpha_2 \frac{\beta_2^2}{\alpha_1^2} (\tan^2 \varphi^{iii} - 1) \end{bmatrix}. \quad (2)$$

Instead of a transmitted, there is a reflected SV wave with amplitude  $B$ , rotated using the right-hand coordinate system. The boundary conditions are the same as for the liquid–solid boundary.

Although the solid–solid boundary transmission/reflection coefficients are not included in the theoretical estimate of the inner–outer core density ratio, we derive them following the same principles that were established in the above derivations (reflecting and refracting  $P$  and SV waves result in four transmission/reflection coefficients). In addition to the amplitudes denoted for the solid–liquid boundary,  $E$  is the amplitude of the reflected SV wave (at an angle  $\varphi^{iv}$ ). The boundary conditions that are used to solve the system of four equations for the solid–solid transition are: (1) continuity of vertical displacements, (2) continuity of tangential stresses and (3) continuity of normal stresses (both  $\sigma_{xx}$  and  $\sigma_{zz}$ ). After a considerable amount of algebra, the resulting equations are

$$\begin{bmatrix} \alpha_1 \tan \varphi & -\beta_1 & -\alpha_2 \tan \varphi^{ii} & \beta_2 \\ -2\alpha_1 \beta_1^2 \rho_1 \tan \varphi & -\beta_1^3 \rho_1 (1 - \tan^2 \varphi^{iv}) & -2\alpha_2 \beta_2^2 \rho_2 \tan \varphi^{ii} & \beta_2^3 \rho_2 (1 - \tan^2 \varphi^{iii}) \\ \alpha_1 \beta_1^2 \rho_1 (\tan^2 \varphi^{iv} - 1) & -2\beta_1^3 \rho_1 \tan \varphi^{iv} & \alpha_2 \beta_2^2 \rho_2 (\tan^2 \varphi^{iii} - 1) & -2\beta_2^3 \rho_2 \tan \varphi^{iii} \\ -(\alpha_1^2 - 2\beta_1^2) \alpha_1 \rho_1 \sec^2 \varphi - 2\alpha_1 \beta_1^2 \rho_1 & 2\beta_1^3 \rho_1 \tan \varphi^{iv} & (\alpha_2^2 - 2\beta_2^2) \alpha_2 \rho_2 \sec^2 \varphi^{ii} + 2\alpha_2 \beta_2^2 \rho_2 & 2\beta_2^3 \rho_2 \tan \varphi^{iii} \end{bmatrix} \begin{bmatrix} B/A \\ C/A \\ D/A \\ E/A \end{bmatrix} = \begin{bmatrix} -\alpha_1 \tan \varphi \\ -2\alpha_1 \beta_1^2 \rho_1 \tan \varphi \\ \alpha_1 \beta_1^2 \rho_1 (\tan^2 \varphi^{iv} - 1) \\ (\alpha_1^2 - 2\beta_1^2) \alpha_1 \rho_1 \sec^2 \varphi + 2\alpha_1 \beta_1^2 \rho_1 \end{bmatrix}. \quad (3)$$

Transmission/reflection coefficients from the above equations could be associated with different branches of body waves, and the system of eqs (1), (2) or (3) can be solved for any liquid–solid, solid–liquid or solid–solid boundary within the Earth. In order to better understand the effects of discontinuities on PKiKP and PcP, we first plot the effects due to transmission/reflection coefficients alone in Figs 1 and 2.

Fig. 1 shows the transmission/reflection coefficients for the ICB and the CMB using the elastic parameters from ak135 model, plotted as a function of the angle of incidence  $90^\circ - \varphi$  (where the angle of emergence was defined as  $0^\circ \leq \varphi \leq 90^\circ$  in eqs 1 and 2). On the liquid side of the CMB, the density of  $9915 \text{ kg m}^{-3}$ , a compressional speed of  $8.000 \text{ km s}^{-1}$ , and the shear wave speed of  $0.000 \text{ km s}^{-1}$  were assumed. On the solid side of the CMB, a density of  $5551 \text{ kg m}^{-3}$ , a compressional wave speed of  $13.660 \text{ km s}^{-1}$ , and a shear wave speed of  $7.281 \text{ km s}^{-1}$  were assumed. On the liquid side of the ICB, the density of  $12\,139 \text{ kg m}^{-3}$ , a compressional wave speed of  $10.289 \text{ km s}^{-1}$ , and a shear wave speed of  $\beta_1 = 0.000$  were assumed. On the solid side of the ICB, a density of  $12\,704 \text{ kg m}^{-3}$ , a compressional wave speed of  $11.043 \text{ km s}^{-1}$ , and a shear wave speed of  $3.504 \text{ km s}^{-1}$  were assumed. There is a critical angle for the solid–liquid case at  $67.8^\circ$ . These ray-theoretical coefficients are independent of frequency but become frequency dependent near grazing incidence of either  $P$  or  $S$  waves on either side of the boundary around  $90^\circ$ , where diffracted/evanescent waves are excited (Richards 1976). In the distance range of the analysis of data that follows, we are far from grazing incidence conditions on both the CMB and inner core–outer core boundaries for both  $P$  waves as well as converted SV waves.

In Fig. 2, the transmission/reflection coefficients for PKiKP (diagram on the left-hand side) and PcP (diagram on the right-hand side) are plotted as a function of epicentral distance. The same model parameters were used as in Fig. 1. Due to interaction with the CMB, the partition of PKiKP energy that is refracted drops with growing epicentral distance. The partition of PKiKP energy that reached the ICB (left-hand diagram) and is reflected, also drops with the epicentral distance, and at about  $70^\circ$ , almost no energy is reflected back to the outer core. At the same time, the reflected portion of PcP from the CMB grows significantly with the epicentral distance and reaches its peak at about  $60^\circ$ . The reverse behaviours of PKiKP and PcP amplitudes as a function of increasing distance illustrates why it is difficult to find high quality observations of PKiKP and PcP from a single earthquake at the same station.

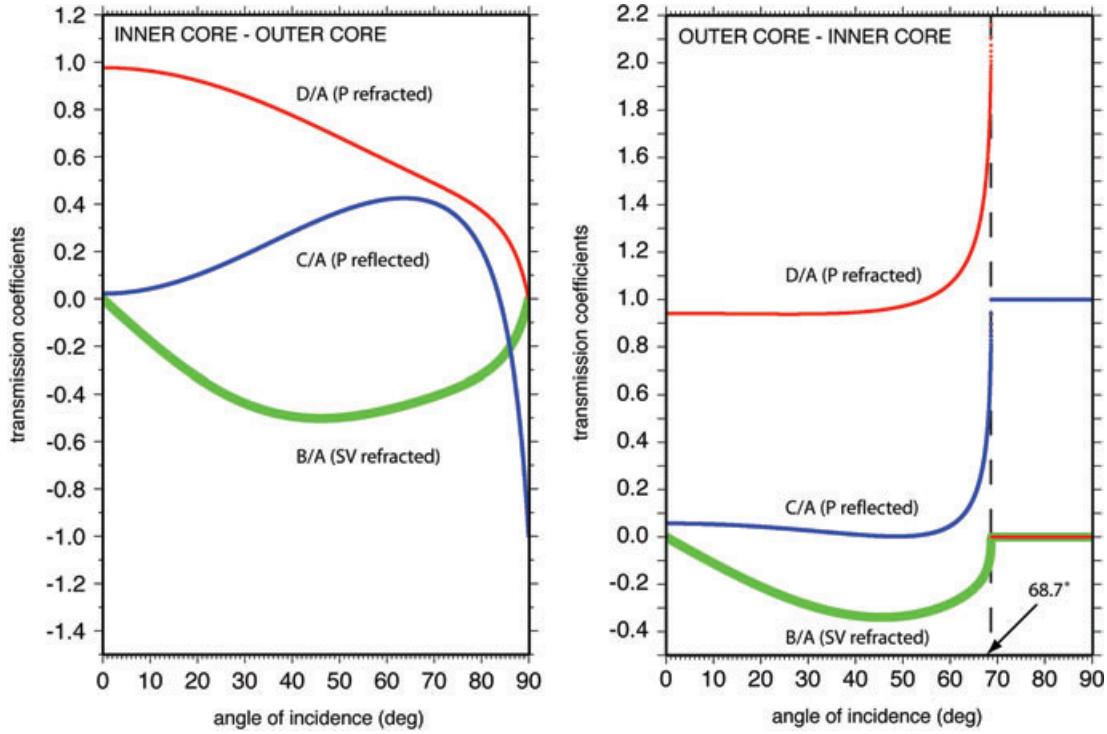


**Figure 1.** Transmission/reflection coefficients for the inner–outer core and core–mantle boundaries as a function of the angle of incidence. The ak135 model is used for the elastic parameters in the surrounding layers. For the notation of the transmission/reflection coefficients, see Section 2.

### 3 THEORETICAL RATIO OF PKiKP AND PcP DISPLACEMENT AMPLITUDES AS A FUNCTION EPICENTRAL DISTANCE

In eqs (1) and (2), the density ratio between liquid and solid appears explicitly. The angles of incidence, reflection and transmission coefficients depend on the elastic parameters and the epicentral distance. PKiKP waves interact with the CMB and the ICB, a total of three times, while PcP waves interact with the CMB only once. Therefore, assuming at near vertical incidence that PcP and PKiKP waves have similar paths through the mantle and that the primary difference between their ray geometries is the PKiKP ray legs in the outer core, the expressions for transmission/reflection coefficients derived in the previous section could be used to calculate theoretical predictions of the inner–outer core density ratio as a function of epicentral distance in a spherically symmetric Earth. At short epicentral distances PcP and PKiKP ray paths are near vertical and obviously nearly similar in the mantle, but increasingly differ in the mantle as distance increases (e.g. Shearer & Masters 1990; Cao & Romanowicz 2004; Koper & Pyle 2004). With the assumption of nearly identical ray paths in the mantle, an expression for PKiKP/PcP displacement amplitude ratio ( $A(\Delta)$ ) as a function of epicentral distance can be written as

$$A(\Delta) = \frac{T_{\text{CMB-D}}(\Delta) R_{\text{ICB}}(\Delta) T_{\text{CMB-U}}(\Delta) \eta_Q(\Delta)}{R_{\text{CMB}}(\Delta) \eta_S(\Delta)}, \quad (4)$$

where  $T_{\text{CMB-D}}(\Delta)$  (D/A in eq. 2) and  $T_{\text{CMB-U}}(\Delta)$  (D/A in eq. 1) are the refraction coefficients of PKiKP wave travelling down and up through the CMB,  $R_{\text{ICB}}(\Delta)$  (C/A in eq. 2) is the reflection coefficient of PKiKP wave at the ICB and  $R_{\text{CMB}}(\Delta)$  (C/A in eq. 1) is the reflection coefficient of PcP wave at the CMB.

In eq. (4),  $\eta_S$  is the PKiKP/PcP ratio geometrical spreading factor, defined using equation 9.69 of Aki & Richards (2002) as

$$\eta_S(\Delta) = \sqrt{\frac{\cos^2(i_{\text{PKiKP}})}{\cos^2(i_{\text{PcP}})} \left( \frac{p_{\text{PcP}}}{p_{\text{PKiKP}}} \right) \left| \left( \frac{dp}{d\Delta} \right)_{\text{PcP}} / \left( \frac{dp}{d\Delta} \right)_{\text{PKiKP}} \right|}, \quad (5)$$

where  $p$  is the ray parameter,  $i$  is the incident angle and  $\Delta$  is the epicentral distance. It is assumed that the source is on the surface.

We assume that of the effect of attenuation suffered by the slightly different ray orientations in the upper mantle can be ignored at distances less than  $30^\circ$ . We also neglect the effect of stronger attenuation in the lowermost mantle where the ray paths of PKiKP and PcP diverge. With these assumptions, the loss of energy of PKiKP compared to PcP can be explained by the difference in attenuation experienced by the additional two ray legs that the PKiKP phase has in the outer core

$$A_{\text{PcP}} = A_{\text{PKiKP}} \exp(\pi \Delta t / QT), \quad (6)$$

where  $\Delta t$  is the two way traveltime of PKiKP waves in the outer core,  $Q$  is the path averaged quality factor in the outer core and  $T$  is the period of PKiKP waves. Although attenuation ( $1/Q$ ) in the middle of the outer core can be confidently set to near zero from the high frequency content of PKiKP (e.g. Cormier & Richards 1976), the possibility of zone of higher attenuation (lower  $Q$ ) has been suggested in a 200–400 km region above the ICB (Zou *et al.* 2008). We examine the effects of lateral variation of a possible strongly attenuating region near the

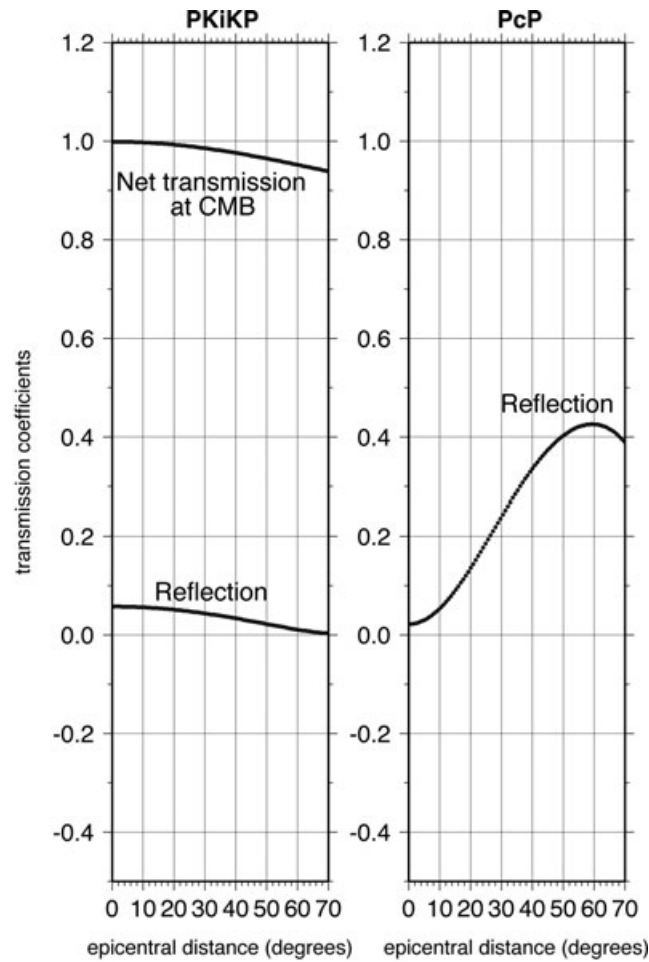


**Figure 2.** Products of transmission/reflection coefficients for PKiKP waves (left-hand side) and the PcP waves (right-hand side) as a function of epicentral distance. The same values for the elastic parameters were used as in Fig. 1.

core–mantle in a related study (Tkalčić *et al.* 2009) The factor  $\eta_Q$  used in eq. (4) is the PKiKP/PcP ratio attenuation correction factor (applied on the double leg of PKiKP in the outer core)

$$\eta_Q = \exp(-\pi \Delta t / QT). \quad (7)$$

Eq. (4) states that using ray theory and the assumption of close proximity of the ray legs in the mantle, the amplitude ratio PKiKP/PcP as a function of epicentral distance is dependent on three factors: (1) the transmission/reflection coefficients at the CMB and the ICB, (2) the geometrical spreading ratio and (3) the elastic attenuation ratio. Eqs (2) and (3) stem from the ray legs of PKiKP in the outer core. It is interesting to discuss the relative contribution of each of these three factors to the amplitude ratio.

Fig. 3 shows the theoretical prediction of the amplitude ratio of PKiKP and PcP waves, when all three contributions mentioned above are combined (black solid line) and when ak135 model is used (Kennett *et al.* 1995). Attenuation specified by  $Q_k = 10\,000$  in the outer core and period  $T = 1$  s are assumed in eq. (7). Including the attenuation in the outer core will have the smallest impact on the theoretical amplitude ratio (light blue solid line for the excluded outer core attenuation; light blue dashed line for the contribution of outer core attenuation only). In fact, the uncertainties of the amplitude ratio measurements exceed the resolution of current outer core attenuation models. Furthermore, varying the period from 1 to 3 s will only have a negligible impact on the theoretical predictions of amplitude ratios, and this impact will be the largest at  $0^\circ$ , changing the prediction from 0.505 to 0.545 (7.3 per cent) and will be nearly zero at  $30^\circ$  or longer epicentral distances. The difference in  $t^*$  accumulated through the mantle has a larger effect than the outer core. Accounting for geometrical spreading will have by far a more dramatic impact on the theoretical curve. Without accounting for geometrical spreading effects, the shape of the amplitude ratio as a function of epicentral distance would remain the same, however the curve would be shifted towards higher theoretical values for the same epicentral distance (red solid line for the excluded effects of geometrical spreading; red dotted line for the contribution from geometrical spreading only). This effect becomes more dramatic for a decreasing epicentral distance. Finally, the largest contribution to the theoretical amplitude ratio comes from the combination of the four transmission/reflection coefficients appearing in eq. (4). It is clear from Fig. 3 that the shape of the theoretical amplitude ratio curve as a function of epicentral distance is controlled mostly by the transmission/reflection coefficients (green dotted line) and that the same function changes dramatically when the effects of energy partitioning at boundaries are excluded (green solid line). If PREM is used instead of ak135, the resulting figure will be nearly identical to Fig. 3, the only difference

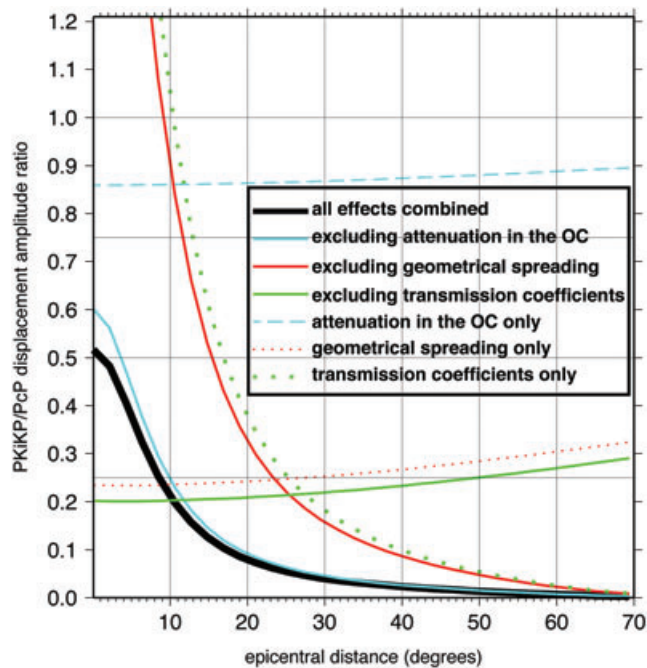


**Figure 3.** Theoretical prediction of the amplitude ratios when only individual contributions (transmission/reflection coefficients, attenuation, geometrical spreading) or two out of the three contributions were considered.

being in the theoretical values being slightly reduced at all epicentral distances (e.g. 0.485 for PREM, as opposed to 0.505 for ak135 near  $0^\circ$  and 0.0385 for PREM as opposed to 0.0408 for ak135 near  $30^\circ$ ). Because the transmission/reflection coefficients have the largest impact on the theoretical amplitude ratios, it is to be expected that these ratios will be very sensitive to the elastic properties near the CMB and the ICB.

#### 4 THEORETICAL DENSITY CONTRAST AT THE ICB AND POTENTIAL SOURCES OF SCATTER IN PKiKP/PcP AMPLITUDE RATIOS

The first density contrast estimate at the ICB was determined finding the intersection of the horizontal line corresponding to the observed PKiKP/PcP amplitude including the attenuation and geometric spreading corrections and the theoretical PKiKP/PcP function of epicentral distance (Bolt & Qamar 1970). A similar diagram is displayed in Fig. 4. The longer the epicentral distance for the same density contrast at the ICB the smaller the theoretical PKiKP/PcP amplitude ratio. According to Bolt & Qamar (1970), if one can read the PKiKP/PcP amplitude ratio from a seismogram recorded at the epicentral distance  $\Delta$ , if the radiation pattern of the source and the earth model are well known, one can then infer the corresponding density contrast at the ICB.

It has been recognized, however, that there exist numerous sources of biases and potential trade-offs in these ratio estimates. Although the ray paths of PKiKP and PcP are nearly identical in the vicinity of the source, care must be taken to avoid computing ratios when both PKiKP and PcP are near a node in the radiation pattern of an earthquake, where amplitude varies strongly with take-off angle and may exhibit some frequency dependent waveform distortion. Koper & Dombrovskaya (2005) showed that the distribution of the radiation pattern corrections was symmetric, with the mean near one (their fig. 8), however according to their estimate there were still about 20 per cent of corrections outside 0.75 and 1.25, which could significantly affect the inferred values of  $\Delta\rho$ . This is not a concern for explosion data, but explosion data are extremely rare in comparison with the number of earthquakes with more complex sources.

Another, potentially very strong, source of error comes from measurements done on the recordings at longer epicentral distances, where the assumption of similar PcP and PKiKP ray paths in the mantle breaks down. One attractive possibility to overcome this latter difficulty is using seismograms recorded at very short epicentral distances. Unfortunately, other sources of errors at short epicentral distances, stemming from the uncertainties in the earth model, preclude straightforward determination of the density contrast at the ICB. One such source of uncertainties is shown in Fig. 5. Depending on the density contrast at the CMB, the theoretical curves for the amplitude ratio as a function of epicentral distance will vary, so that a larger density contrast at the CMB will produce a smaller PKiKP/PcP amplitude ratio. This is to be expected because a larger density contrast at the CMB will result in a larger partition of the PcP energy reflected from the boundary. For example, for an epicentral distance of  $10^\circ$ , the theoretical amplitude ratios increase from 0.15 to 0.35 for a density contrast decrease from 5000 to 4000  $\text{kg m}^{-3}$  at the CMB. Near the epicentral distance of  $20^\circ$ , the effect ceases to be serious. In other words, if there is a density contrast variation of 1000  $\text{kg m}^{-3}$  at the CMB, the expected scatter of amplitude ratios would be confined to the area bounded by the curves in Fig. 5. All the theoretical curves in Fig. 5 are computed assuming the ak135 model.

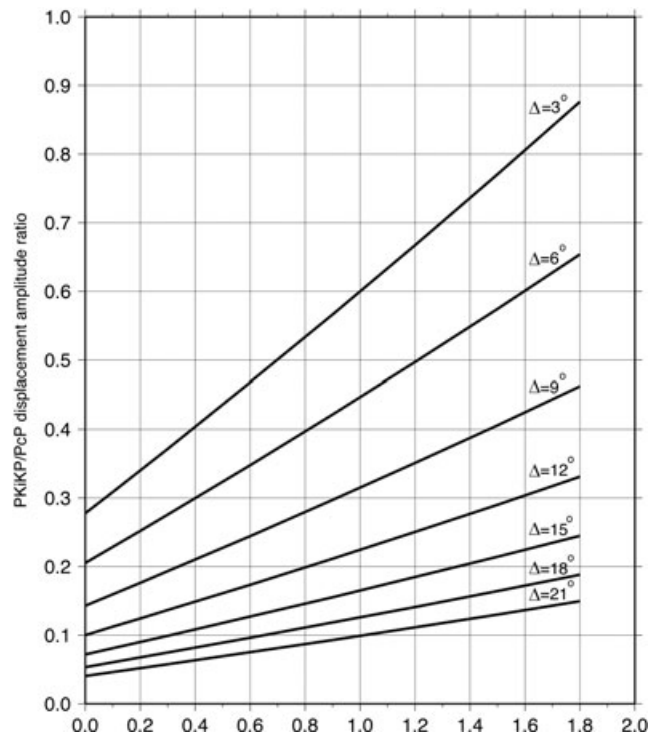


Figure 4. PKiKP/PcP amplitude ratios versus ICB density contrast for different epicentral distances.

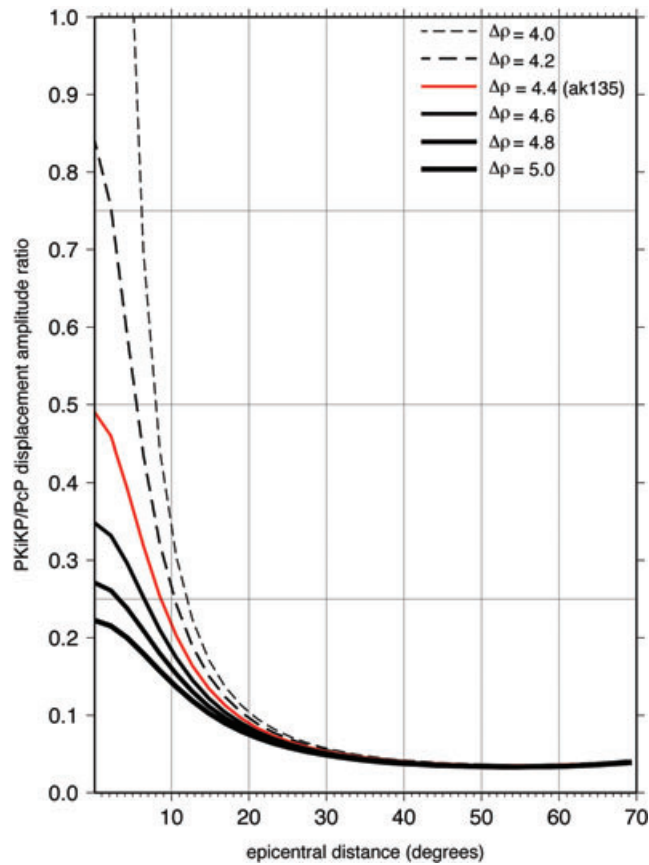
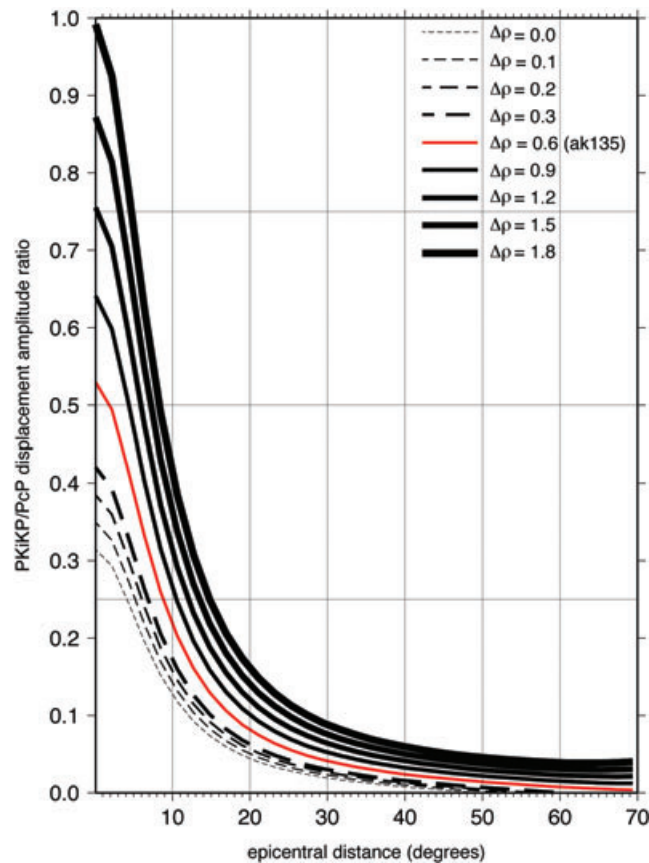


Figure 5. PKiKP/PcP amplitude ratio as a function of epicentral distance for varying density contrast at the CMB as indicated in the legend. The ak135 model was assumed.



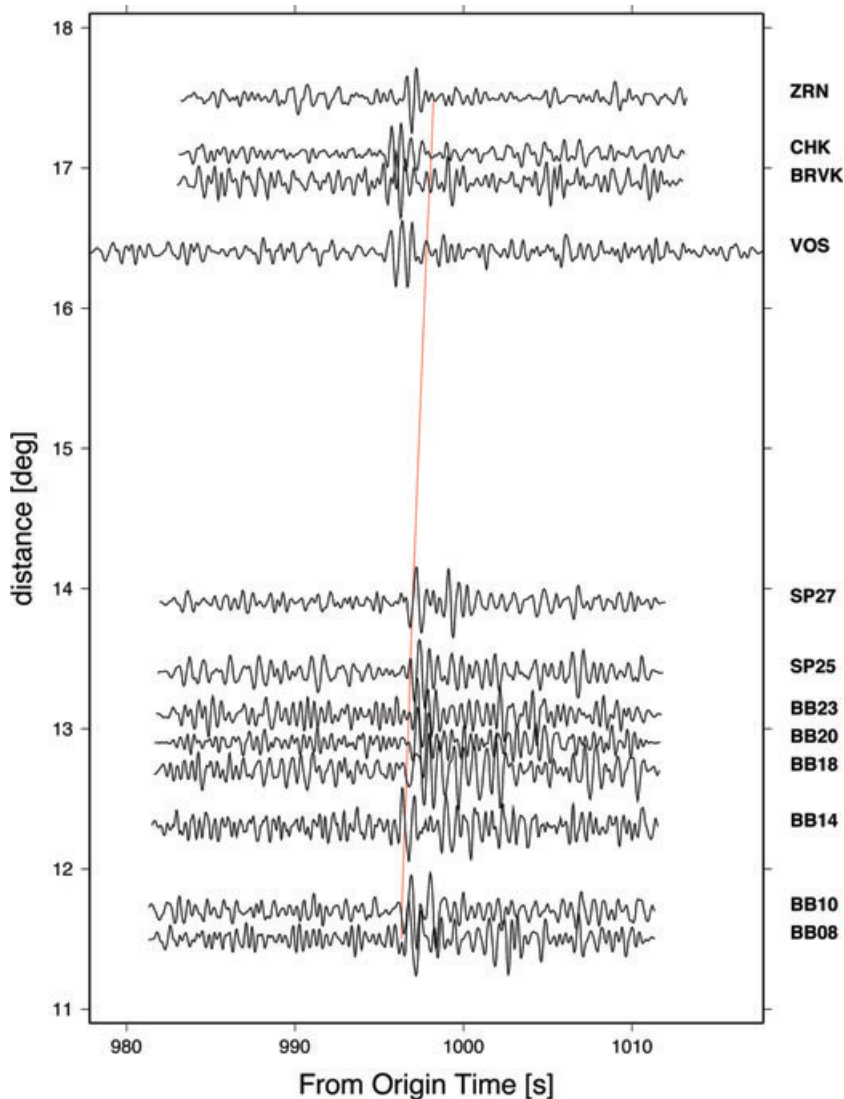
**Figure 6.** PKiKP/PcP amplitude ratio as a function of epicentral distance for varying density contrast at the ICB as indicated in the legend. The ak135 model was assumed.

Fig. 6 shows the theoretical curves of amplitude ratio as a function of epicentral distance for varying density contrast at the ICB, from 0 to  $1800 \text{ kg m}^{-3}$ , assuming all other elastic parameters from ak135 model. As expected, the amplitude ratio now increases with an increase in the density contrast at the ICB, as a result of a larger partition of the PKiKP energy to the outer core by reflection from the ICB. If there is a lateral variation in the density contrast at the ICB (from 0 to  $1800 \text{ kg m}^{-3}$ ), there will be a scatter of amplitude ratios confined to the area bounded by the curves shown in Fig. 6. The scatter will be dominant at short distances, but it will persist at long epicentral distances as well, unlike the case for lateral variations of the density contrast at the CMB. Koper & Pyle (2004) showed that uncertainty in seismic velocities near the boundary is another source of errors in estimating the density contrast near the CMB.

## 5 OBSERVATIONS OF PKiKP AND PcP WAVES

A routine way of measuring amplitudes of seismic phases is to find an appropriate bandpass filter in the time-domain, and read peak-to-peak amplitude of the most-pronounced cycle, most frequently on the vertical component. The uncertainty could then be estimated by measuring the amplitude of the seismic phase of interest on a number of traces (from different events) for the same instrument. The observations of seismic phases such as PKiKP, however, are sparse, and it is not likely that they will be recorded multiple times at the same station, except for a fixed path for multiple explosions. Furthermore, this would implicitly involve another kind of uncertainty, as different size events will have to be normalized by their amplitude. Therefore, it is demonstrated here how to use the observations of PKiKP waves from a single source, and at the same time account for the seismic noise to express the uncertainty of the amplitude measurements.

In addition, the radiation pattern of the source and different structural effects (attenuation) along each source–receiver path will have profound influence on the amplitude measured at the receiver. To get a robust measurement of absolute amplitudes, one has to consider those events for which the size and radiation pattern are known with some certainty and one has to take into account the possible effect that the attenuation along the path can have on the amplitudes. The radiation patterns of most nuclear explosions are theoretically isotropic (equal  $P$  amplitude radiated in all directions) and, in the worst case scenario of tectonic release or significant spall, far less complicated than those for earthquakes dominated by the double-couple force representation of slip on a fault plane. This makes them a logical choice for PKiKP- and PcP-related absolute amplitude measurements, if a careful procedure in picking peak-to-peak amplitude is used. Fig. 7 demonstrates an example of excellent quality velocigrams of PKiKP waves observed at the epicentral distances between  $10^\circ$  and  $20^\circ$  from a nuclear explosion at the Lop Nor test-site in Xinjiang Province, China. When the waveforms are filtered with the same filter (1.0–3.0 Hz bandpass in Fig. 7),



**Figure 7.** Observations of the PKiKP waves on the velocity seismograms of various stations in Asia for a Lop Nor test-site explosion from 1994 October 7. The theoretical traveltime prediction of PKiKP from the ak135 model is shown by solid line.

some of the recorded PKiKP arrivals are simple, and some are followed by a secondary arrival and a more complex coda. There are a number of similarly well-recorded PcP waves for the same explosion, some of which will be presented in later figures.

## 6 SEISMIC NOISE USED AS THE UNCERTAINTY MEASURE

Recordings from the nuclear explosion at the Lop Nor test site recorded at various stations in Asia were chosen for further analysis. The main assumption is that this event will have a uniform isotropic radiation of  $P$  waves and that the amplitude of PKiKP and PcP waves observed at different stations will decay only as a function of distance. Among other things, this assumption allows a straightforward procedure for a comparison of the observed and theoretical predictions for the amplitude as a function of distance. Using the SAC software package ([www.lnl.gov/sac](http://www.lnl.gov/sac)) the instrument response of each station was removed, after which the velocity amplitudes (expressed in  $\text{nm s}^{-1}$ ) were measured. Note that the examples demonstrating the use of noise to estimate the uncertainty in this section use ground velocities, although the measurements of PKiKP and PcP amplitudes for the purpose of estimating the density contrast at the ICB are carried out using displacements, and this will be demonstrated in later figures. Furthermore, an example with a rather challenging observation of PKiKP at large epicentral distance for which the reported PKiKP phases in the literature are extremely rare, was chosen to demonstrate the use of noise in the estimation of the uncertainties. It is important to note that the noise preceding PKiKP or PcP waves consists of a combination of teleseismic and event-generated (scattered wave) noise. Both cases of unfiltered and bandpass filtered waveforms are considered.

In order to demonstrate how the noise might impact amplitude measurements, we used an unfiltered seismogram with clear  $P$ -wave arrivals as ‘the signal’, and we showed how the noise preceding the PKiKP phase combines with the  $P$ -wave signal (Fig. 8) by looking at the influence of changing noise on the amplitude pattern. The procedure is as follows: the selected station is BGCA, at  $71.9^\circ$  away from

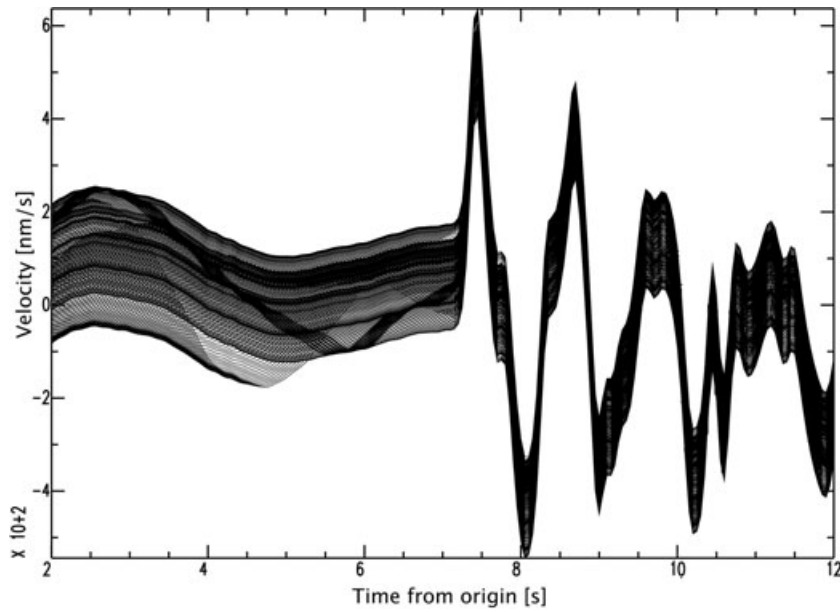


**Figure 8.** The superposition of seismic noise on the *P*-wave signal. 200 consecutive, 14-s-long sliding windows of noise time-series are calculated by shifting the time-series by one sample towards earlier time and are then added to the *P*-wave signal. The records are unfiltered. Only 10 s of the time-series are shown for clarity.

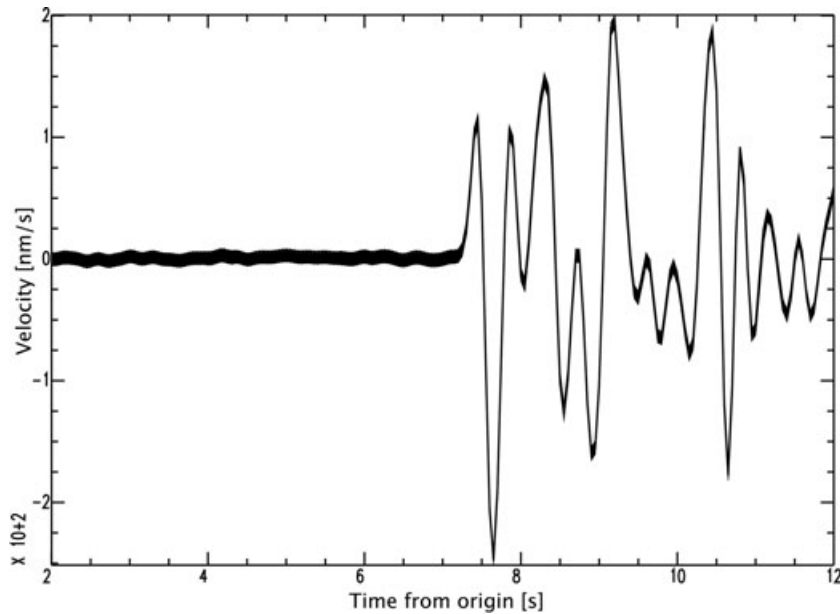


**Figure 9.** Same as in Fig. 8, but the waveforms are filtered with a Butterworth bandpass filter of 1.3–3.8 Hz prior to the superposition of noise to the *P*-wave signal.

the source. After the instrument response is removed, displacements could be used, or they could be differentiated to produce velocities in  $\text{nm s}^{-1}$ . The onsets of *P* and PKiKP waves were then identified and the 14-s-long time-series with *P* onset in the centre were excised. The same was repeated for PKiKP waves, but the 28-s-long time-series preceding the PKiKP onsets were employed. In this example, the sampling rate is 20 samples per second, and a rather conservative approach was taken when using a total shift in time of 10 s, resulting in 200 consecutive, 14-s-long noise time-series. These sliding windows of noise time-series are calculated by shifting the time-series by one sample towards earlier time. The noise time-series are then added to the *P*-wave signal.

In Fig. 8, 200 resulting (unfiltered) waveforms are shown centred on the *P*-wave onset. The peak-to-peak amplitude of *P* waves varies between 882 and 1019  $\text{nm s}^{-1}$ . It is important to keep in mind that the new amplitudes contain the microseismic noise twice, however in this example we are only interested in observing how the peak-to-peak amplitude measurement varies.

In the next step, a number of bandpass filters were tested with a systematic search over width and corner frequencies. The filter producing the best signal to noise ratio was chosen. Fig. 9 shows the same data as Fig. 8, but for bandpass filtered waveforms between 1.3 and

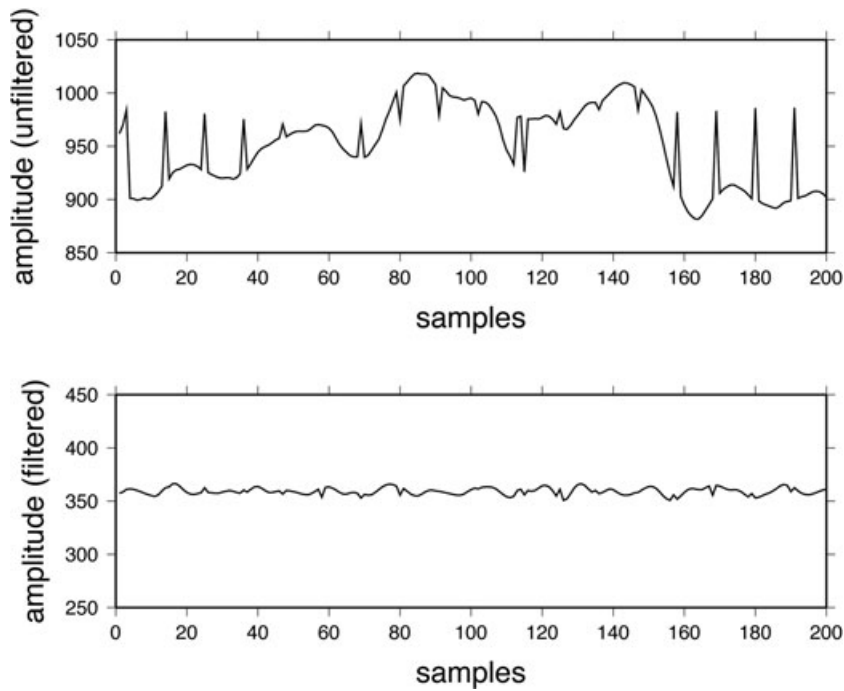


**Figure 10.** The variation of maximum peak-to-peak amplitude measured for the unfiltered waveforms shown in Fig. 8 (top panel) and for the filtered waveforms shown in Fig. 9 (bottom panel).

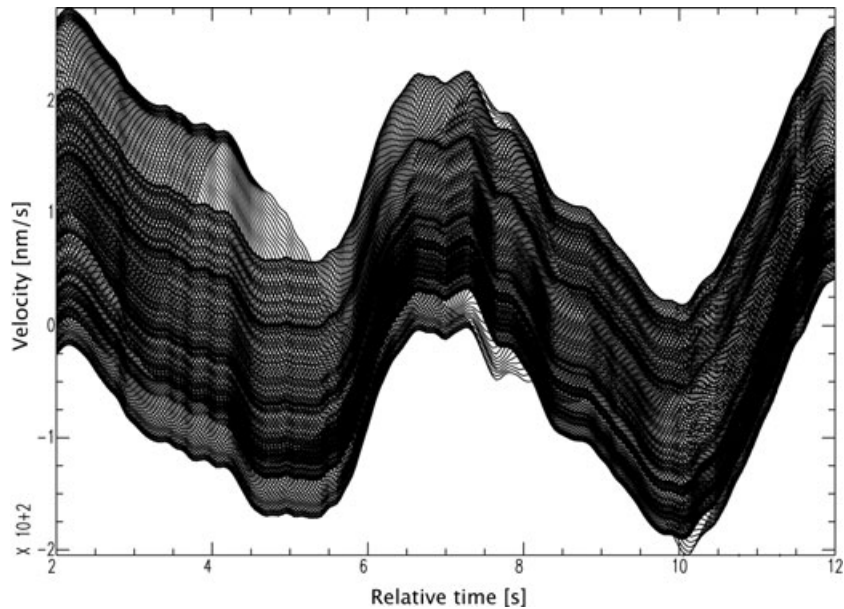
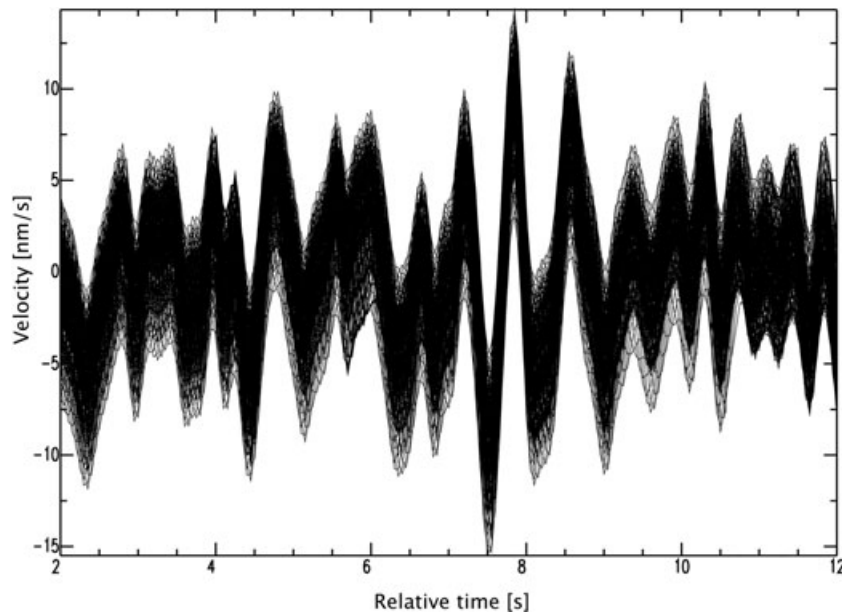


**Figure 11.** The subtraction of unfiltered seismic noise preceding the PKiKP waves from the PKiKP-wave signal recorded at station BGCA for the Lop Nor explosion from 1994 October 9. 200 consecutive, 14-s-long sliding windows of noise time-series are calculated by shifting the time-series by one sample towards earlier time and are then subtracted from the PKiKP-wave signal. Only 10 s of the time-series are shown for clarity.

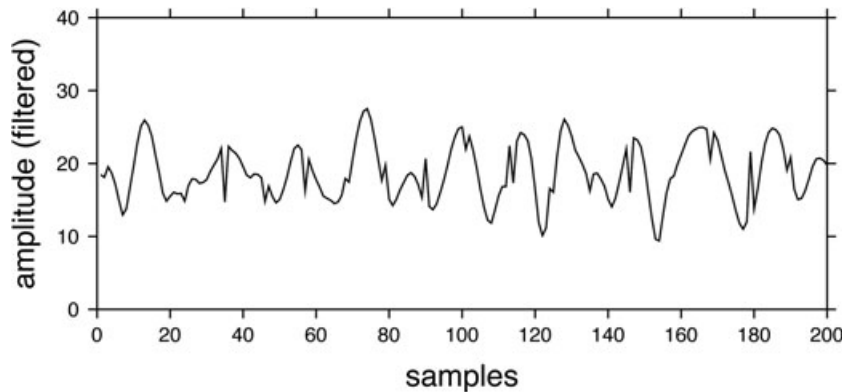
3.8 Hz, which was selected as the optimal filter. Much less variation is observed for the filtered waveforms because the microseismic noise has been optimally filtered out. The amplitude of the  $P$  waves now varies between 351 and 366 nm/s. This variation represents about a 4 per cent variation from the average amplitude.

Fig. 10 shows the variation of maximum peak-to-peak amplitude as a function of shift in samples in noise patterns for unfiltered (top) and filtered (bottom) waveforms. Vertical scales are equal, and it is evident that there is much less variation in the resulting waveforms for the bandpass filtered waveforms when the microseismic noise is suppressed. This figure reveals a pattern of noise with a dominant period of  $T \approx 30$  samples and illustrates how the noise is superposed to the signal in the time domain.

In the next experiment, we consider a realistic case, where instead of  $P$  waves, we estimate the variation of maximum peak-to-peak amplitudes of PKiKP waves for the same event and station that were shown in Figs 11 and 12. The procedure is very similar to the one



**Figure 12.** Same as in Fig. 11, but the waveforms are filtered with a Butterworth bandpass filter of 1.3–3.8 Hz prior to the subtraction of noise from the PKiKP-wave signal.



**Figure 13.** The variation of maximum peak-to-peak amplitude measured for the filtered waveforms shown in Fig. 12.

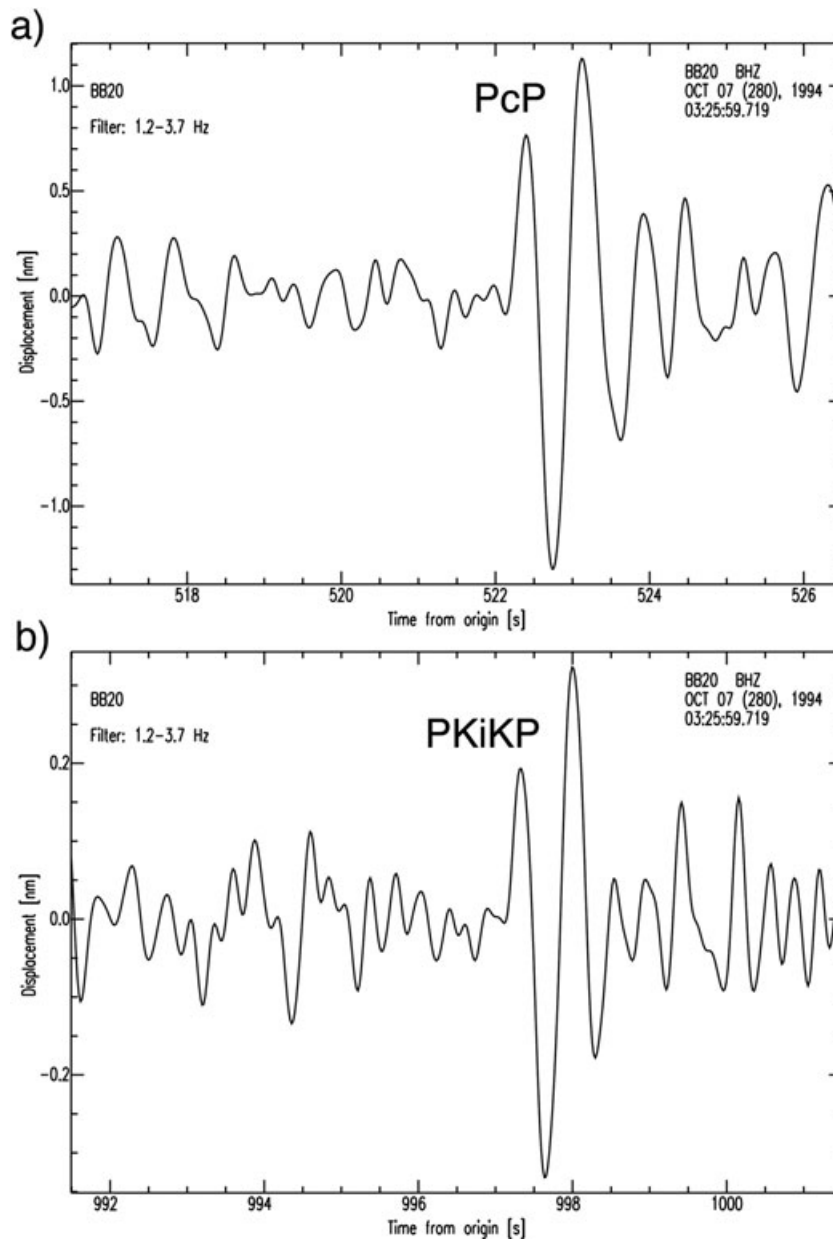
described above for  $P$  waves, but instead of adding, we now subtract the noise preceding PKiKP waves from the PKiKP signal. Fig. 11 shows the resulting 200 waveforms for the case where waveforms are unfiltered and Fig. 12 is the case with bandpass filtering.

Fig. 13 shows the variation of the estimated PKiKP amplitudes using the PKiKP preceding noise for the case when the waveforms are bandpass filtered. As the noise gets subtracted and shifted around, the peak-to-peak amplitude measured on the same part of the waveform (from minimum to maximum) will oscillate around  $18.45 \text{ nm s}^{-1}$  (the value measured without subtracting the noise). This experiment demonstrates that the maximum observed amplitude is  $27.5 \text{ nm s}^{-1}$  for the case of constructive interference with the noise. As for the minimum, although the minimal estimate peak-to-peak amplitude using this method is  $9.4 \text{ nm s}^{-1}$ , PKiKP onsets would not be identified, because in that case they would be buried in noise.

In what follows, we will apply this method to a number of stations on which PcP and PKiKP waves were observed, to measure their amplitude as a function of epicentral distance.

## 7 PKiKP AND PcP AMPLITUDE MEASUREMENTS

The method described in the previous section was applied to a number of seismograms to measure the absolute PKiKP and PcP amplitudes. For demonstration purposes, we selected station BB20 at a relatively short epicentral distance ( $12.7^\circ$ ). The filter that emphasizes PKiKP is carefully selected in a systematic way, testing a number of consecutive bandpass filters with various widths. A Butterworth bandpass filter with corner frequencies 1.2 and 3.7 Hz was selected as an optimal filter that emphasizes both PcP and PKiKP signals. The resulting waveforms were inspected in both time domain and as spectrograms. The filtered PcP and PKiKP waveforms are shown in Figs 14(a) and (b) for comparison. The waveforms are similar and of extraordinary quality, and that ensures not only an unambiguous identification of the phases, but also a high quality of the amplitude ratio measurements. The shape of PcP and PKiKP arrivals is very similar, although PKiKP



**Figure 14.** Bandpass-filtered ground displacements recorded at station BB20 using an optimal filter of 1.2–3.7 Hz for the event from Fig. 7. Clear observations with similar waveforms of the PcP and PKiKP waves are visible.

generally contains somewhat higher frequencies than PcP, which could be a result of differences in scattering and intrinsic attenuation that takes place along the uncommon part of the ray paths, most likely near the CMB or the ICB.

An ensemble of PcP and PKiKP waveforms with subtracted noise is shown in Figs 15(a) and (b). Note that the sampling rate for BB and ST stations is 50 sps (40 sps for ZRN and VOS); therefore in order to be consistent with the previous example, where a superposition of the noise to the signal with a shift of 10 s was considered, 500 waveforms were calculated here (400 for ZRN and VOS).

The measurements of PcP and PKiKP peak-to-peak amplitudes, including the median and the maximum deviation from the median are done using the shifting algorithm, and the ratios and the corresponding errors are calculated. Medians are more adequate measures than the arithmetic means, as they will not be biased towards the extreme values. The errors are estimated using the following procedure.

Let  $A$  be the median peak-to-peak amplitude of PcP (500 measurements in the procedure described above) and  $B$  the median peak-to-peak amplitude of PKiKP waves (also 500 measurements) and let  $\Delta A$  and  $\Delta B$  be maximum absolute departures from the median for the PcP and PKiKP peak-to-peak amplitudes, respectively (these symbols are not related to those in eqs 1 and 2). Table 1 shows these measurements for each recording for which PcP and PKiKP were clearly observed. For example, for station BB20, peak-to-peak PcP displacement amplitude measured from the record shown in Fig. 14(a) is 2.43 nm. The range of peak-to-peak amplitudes measured when noise is combined with the same signal (Fig. 15a) is from 1.76 to 3.08 nm, and the median is 2.45 nm. The maximum absolute departure from the median is 0.67 nm. Similarly, for the PKiKP displacement amplitude signal, the median of 0.67 nm and the maximum absolute departure from median of

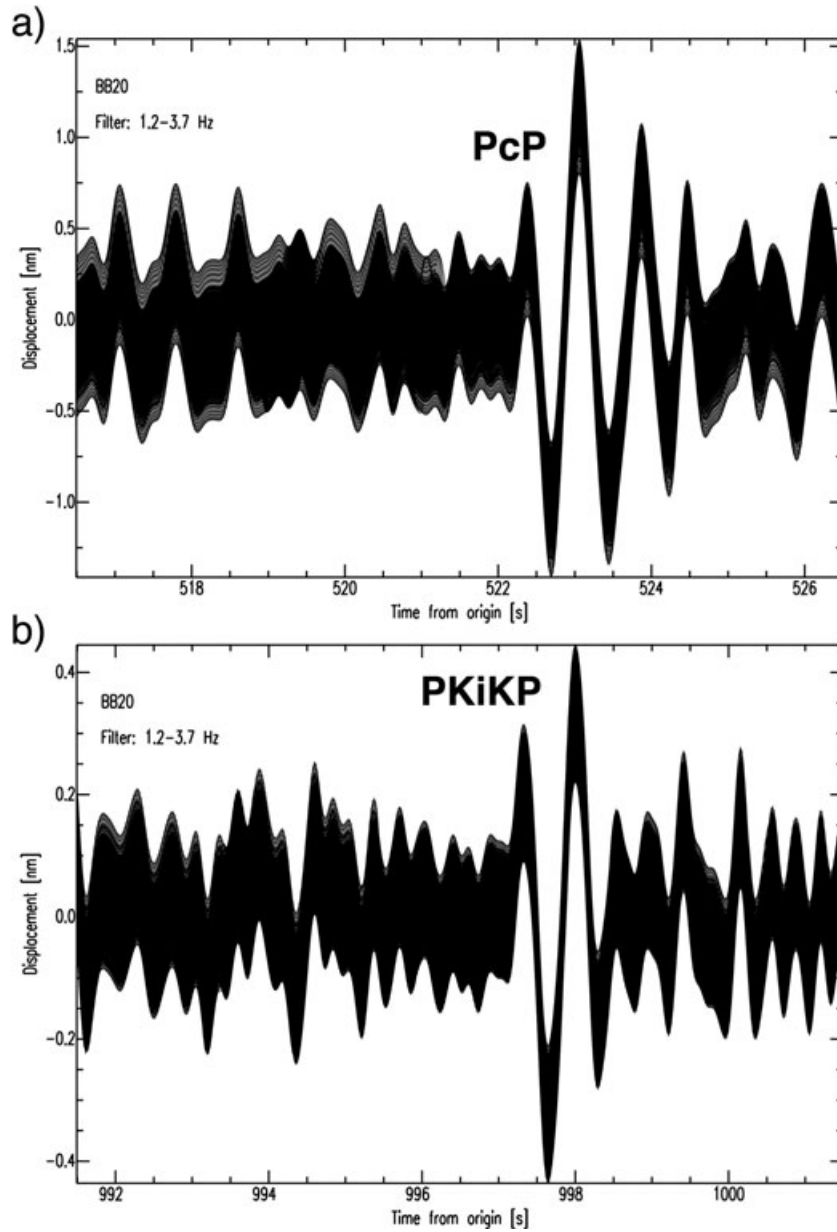


**Figure 15.** The subtraction of bandpass-filtered (1.2–3.7 Hz) seismic noise preceding the PKiKP waves from the PKiKP-wave signal recorded at station BB20 for the event from Fig. 7. 500 consecutive, 14-s-long sliding windows of noise time-series are calculated by shifting the time-series by one sample towards earlier time and are then subtracted from the bandpass-filtered PKiKP-wave signal. Only 10 s of the time-series are shown for clarity. Compare with Fig. 14.

0.18 nm were obtained. The PKiKP/PcP ratio  $u$  is defined by

$$u = \frac{A}{B}. \quad (8)$$

The corresponding error  $\Delta u$  is defined by

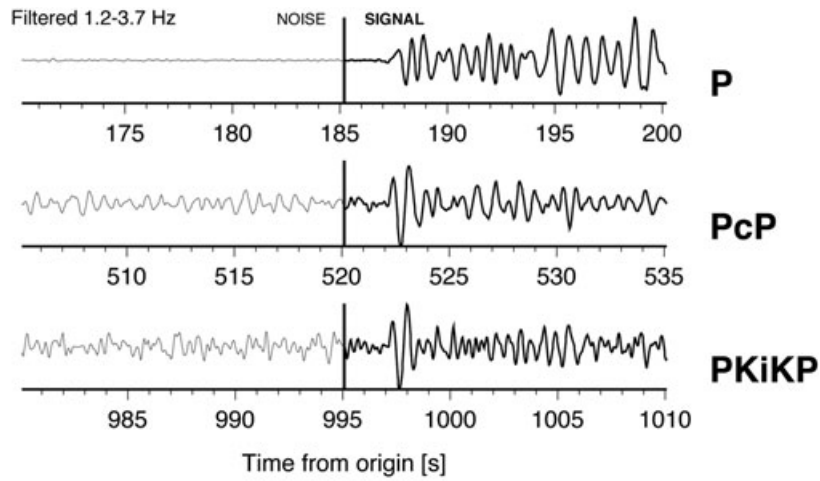
$$\Delta u = \frac{1}{B^2} (B\Delta A + A\Delta B). \quad (9)$$

For station BB20, this gives the amplitude ratio  $u \pm \Delta u$  of  $0.27 \pm 0.15$ .

Fig. 16 demonstrates P, PcP and PKiKP displacement seismograms recorded at station BB20, for an optimal bandpass filter of 1.2–3.7 Hz.  $P$  waveforms at this short distance of  $12.9^\circ$  are complex, as the  $P$  wave interacts with and is scattered by laterally varying first-order discontinuities and strong heterogeneity concentrated in the crust and upper mantle. PcP and PKiKP waves leave the focal sphere at a significantly different angle to the  $P$  waves, traversing the heterogeneous crust and upper mantle over only a very short, nearly coincident, path that will affect both waveforms by essentially equal perturbations due to crustal backscattering and attenuation. The vertical bars in Fig. 16 represent the boundary between ‘signal’ and ‘noise’ windows used in the amplitude measurements method described above. It is clear that the frequency content

**Table 1.** PcP and PKiKP amplitude measurements ( $A_{MED}$ ,  $B_{MED}$ ), the PKiKP/PcP amplitude ratios ( $A/B$ ) and the corresponding uncertainties ( $\Delta A/B$ ) used in this study. Also shown are direct amplitude measurements in the time domain ( $A_{PcP}$  and  $B_{PKiKP}$ ), as well as the minimum and maximum uncertainty estimate taking noise into account ( $A_{MIN}$ ,  $A_{MAX}$ ,  $B_{MIN}$ ,  $B_{MAX}$ ). All peak-to-peak measurements are performed between precisely the same minimum and maximum oscillation on the waveforms.

Station name	Dist. ( $^{\circ}$ )	$A_{PcP}$ (nm)	$A_{MIN}$ (nm)	$A_{MAX}$ (nm)	$A_{MED}$ (nm)	$\Delta A_{PcP}$ (nm)	$B_{PKiKP}$ (nm)	$B_{MIN}$ (nm)	$B_{MAX}$ (nm)	$B_{MED}$ (nm)	$\Delta B_{PKiKP}$ (nm)	$A/B$	$\Delta A/B$
BB10	11.69	11.20	6.95	14.51	11.56	4.61	3.04	2.22	3.90	3.11	0.89	0.27	0.19
BB36	11.88	31.16	23.05	41.23	30.89	10.34	6.41	2.05	12.40	6.60	5.80	0.21	0.26
BB18	12.68	14.89	8.83	21.47	15.08	6.39	2.45	1.68	3.66	2.52	1.14	0.17	0.15
BB20	12.88	2.43	1.76	3.08	2.45	0.67	0.66	0.49	0.84	0.67	0.18	0.27	0.15
BB23	13.12	39.02	32.36	46.15	39.88	7.52	4.87	3.43	7.78	5.35	2.43	0.13	0.09
SP25	13.41	13.86	7.36	20.37	14.62	7.26	2.12	1.56	2.92	2.15	0.77	0.15	0.13
VOS	16.37	41.62	20.77	68.55	44.85	24.08	3.79	2.44	5.38	3.85	1.53	0.09	0.08
ZRN	17.49	431.71	244.19	661.36	449.62	211.74	30.58	16.90	40.43	31.51	23.52	0.07	0.09



Station: BB20 Elat: 41.613 Elon: 88.759 Distance: 12.878

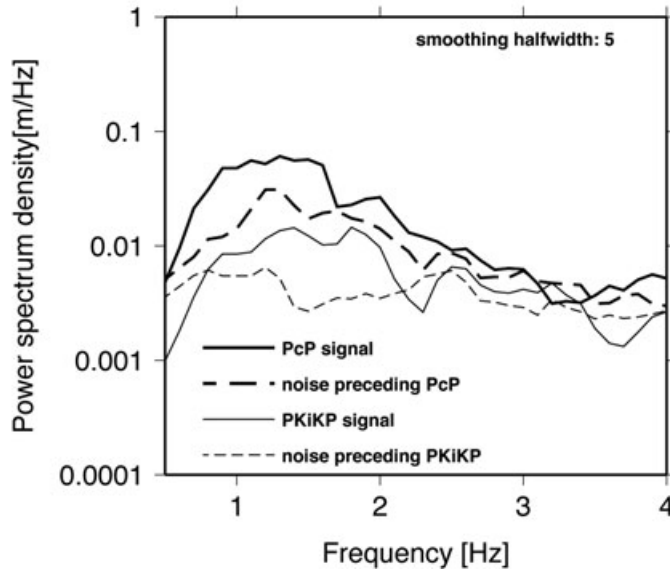


**Figure 16.** (Top panel) The  $P$ , PcP and PKiKP bandpass-filtered waveforms recorded at station BB20 showing the separation between the signal and noise windows used in the measuring procedure described in Section 7; (Bottom panel) Power spectrum density for the PKiKP signal (thin solid line), the PcP signal (thick solid line), and noise (dashed lines).

of the PKiKP waveform is different from the PcP waveform, in that it contains higher frequencies. This is true for the entire record and not only for the PKiKP coda. The amplitude spectra in Fig. 16 illustrate how signal relates to noise for PKiKP and PcP waves. They are slightly smoothed, but only after the measurements in the time domain are done. Measurements in the frequency domain are more challenging and the signal stays above the noise over a range of frequencies suitable for such analysis on rare occasions.

## 8 DISCUSSION OF RESULTS

The absolute amplitudes are shown as a function of epicentral distance in Fig. 17 for the measurements reported in Table 1. These measurements are carefully selected data of the highest quality, where possible spurious effects from radiation pattern and differences in ray paths have been eliminated. Both PcP and PKiKP arrivals were clearly identified and there was no interference with other seismic phases. Median values of the peak-to-peak amplitude ratios including the contribution of seismic noise (for 500 independent measurements) are shown with diamonds. The uncertainty estimates determined using the eq. (9) are shown with error bars. Theoretical values corresponding to increasing density contrasts using the elastic parameters from ak135 model are shown with lines of increasing thicknesses. In Fig. 17(a), a range of theoretical density contrasts at the CMB is shown assuming that the density contrast at the ICB from the ak135 model is accurate. In Fig. 17(b), the same is shown for the theoretical density contrast at the ICB, assuming that the density contrast at the CMB from the ak135 model is accurate. These two figures are shown to emphasize a well-known trade-off that exists between the variation of impedance properties (densities and velocities) at the two boundaries and the resulting ICB density contrast estimate (see also Koper & Pyle 2004 for a discussion). Clearly, the conclusions about one boundary will bear on the assumptions made about another. This is at least as serious a challenge as identifying PcP and PKiKP phases from the events with known radiation pattern and minimal ray paths differences in the mantle.

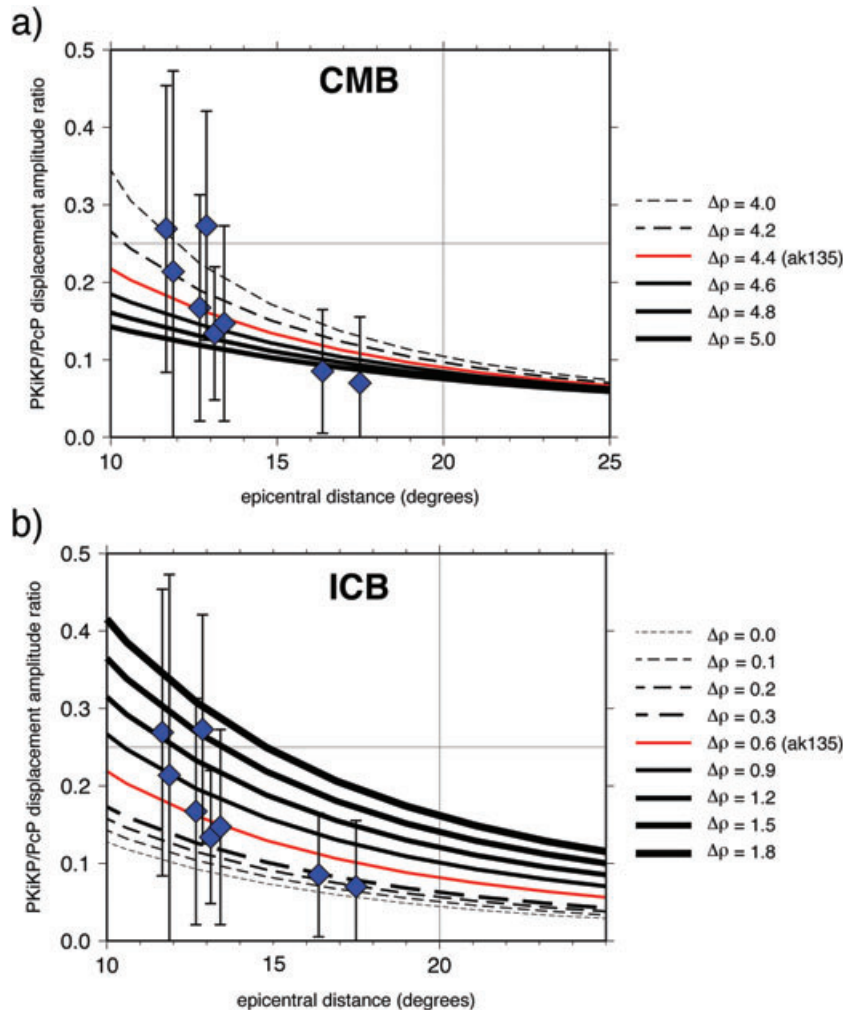


**Figure 17.** PKiKP/PcP amplitude measurements and their uncertainties from Table 1 (the median values are shown by diamonds, and the uncertainties are shown by error bars) plotted as a function of epicentral distance for: a varying density contrast at the ICB (top panel) and the CMB (bottom panel). Theoretical values are identical to those used in Figs 5 and 6.

From Fig. 17, it is clear that the observed amplitude ratios do not lie on a single curve predicted by the theory and assumptions made about Earth. Given the number and nature of assumptions, this is not surprising. The difference of PcP and PKiKP ray paths through the mantle, including attenuation effects has always been a serious problem, which we try to address measuring amplitudes recorded at a very short epicentral distance. The varying radiation pattern has already been mentioned, and it is a well-known source of uncertainty. It should be kept in mind that the published global CMT solutions are not 100 per cent accurate. Even a nuclear explosion considered here for the simplicity of the source physics and as means of achieving a maximum possible accuracy might have a more complex radiation pattern. Ray theory has a number of limitations itself, but one of the fundamental assumptions that is implicitly included in the eqs 1 and 2 are the boundary conditions employed. It is unrealistic to expect that ideal boundary conditions will always be met for major solid–liquid and liquid–solid boundaries within Earth, and as shown in Fig. 3, transmission/reflection coefficients derived from these assumptions play the most significant part in the theoretical predictions.

The group of measurements between  $11^\circ$  and  $14^\circ$  do not reveal information about a possible lower bound of the ICB density contrast as the lower bound of uncertainties falls below  $0 \text{ kg m}^{-3}$ . They increase, however, the constraints on the upper bound of the ICB density contrast. When the uncertainty estimates are not taken into account, these values favour a much lower ICB density contrast than the estimate of  $1800 \text{ kg m}^{-3}$  (Bolt & Qamar 1970) and  $1330\text{--}1660 \text{ kg m}^{-3}$  (Souriau & Souriau 1989), and favour values close to those of ak135 and PREM. When the uncertainties are included, the ICB density contrasts above  $1100 \text{ kg m}^{-3}$  are excluded based on one of the measurements. This confirms recent results (e.g. Masters & Gubbins 2003; Cao & Romanowicz 2004; Koper & Pyle 2004). The uncertainties for three of the measurements, however, extend well above the theoretical estimate for  $1800 \text{ kg m}^{-3}$ . Therefore, the impact of seismic noise on the estimation of amplitude ratio measurements and uncertainties seems to be a likely candidate to explain at least a part of high values estimated by Bolt & Qamar (1970) and Souriau & Souriau (1989), and thus, the discrepancy in published seismological results.

The two measurements near  $16^\circ$  and  $17^\circ$  (at VOS and ZRN, Fig. 7) favour a low ICB density contrast, such as one proposed in Koper & Pyle (2004) and inferred in modelling of Gubbins *et al.* (2008). Such a relatively small density contrast sampled by the body waves agrees well with a model shown to be compatible with geodynamic constraints. This argues in favour of a denser layer at the bottom of the outer core (F region), so that the net density contrast at the boundary is smaller (sampled by the body waves), while the net density contrast between the outer core above the F region and the inner core is larger (sampled by normal modes). Zou *et al.* (2008) recently hypothesized smaller  $Q$  values in that layer.

Although the median values are small, we cannot, however, exclude higher values based on the uncertainties introduced by the consideration of seismic noise. Nonetheless, the upper bounds of the uncertainties confirm that  $1100\text{--}1200 \text{ kg m}^{-3}$  is likely to be the upper bound value for the ICB density contrast inferred from body waves, if an ak135-like CMB contrast is assumed. One possibility is that an apparent shift towards lower density contrast for these two measurements might be due to a different sampling location at the ICB. In that case, such a low contrast in density might reveal sampling of less-solidified regions of the top layer of the inner core or a lateral variation in inner core texture, such as one proposed by Cormier (2007), although on a short scale. Interestingly, the PKiKP waveforms at both VOS and ZRN are simple. Another possibility that would explain the small density contrast measurements at these two stations that cannot be excluded is that the CMB portion sampled by these two paths undergoes a larger density jump, which would result in a more efficient reflection, thus reducing the PKiKP/PcP amplitude ratio. This would more likely be an effect of a reduced density on the mantle side. The corresponding PKiKP at the CMB would not necessarily be affected by the same change in density contrast as the PKiKP zone of sensitivity is well separated from that of the PcP. Apart from uncertainties in densities, variations in compressional velocity contrast at the ICB and CMB could also effect theoretical density contrast estimates (e.g. Koper & Pyle 2004). For example, a theoretical PKiKP/PcP ratio is smaller if the P velocity contrast at the CMB or ICB is smaller.

It is not clear yet why the amplitude ratios at smaller epicentral distances display a larger scatter, but it is predicted that they will be more sensitive to the density and  $P$ -wave velocity ratio at these distances. This behaviour is not likely to be explained by the simultaneous sensitivity of the PcP and PKiKP waves to the same structure at the CMB, as the Fresnel zones at these epicentral distances are almost constant and smaller than the separation between the PcP and PKiKP piercing points. Therefore, a mechanism where, for example, the PcP and PKiKP are affected by a common structure at the CMB, in a way that the PcP waves are not efficiently reflected, while the PKiKP waves are efficiently transmitted through the boundary is excluded.

## 9 CONCLUSIONS

Ray theory was utilized to derive transmission and reflection coefficients at the major boundaries of Earth from ground displacements and amplitudes of PcP and PKiKP waves. This development aids a comparison between the theoretical and observed amplitudes on the displacement seismograms. It is clear from previous studies (Bolt & Qamar 1970; Souriau & Souriau 1989; Shearer & Masters 1990; Masters & Gubbins 2003; Cao & Romanowicz 2004; Koper & Pyle 2004) that the uncertainty in amplitude measurements and the way that uncertainty is reported can present a critical source of variations in the estimated values of the ICB density contrast. An important source of uncertainty in absolute amplitude measurements is seismic noise. The impact of noise was not previously studied extensively enough on PKiKP absolute amplitudes apart from the conclusion that, most of the time, PKiKP gets buried in noise and is therefore difficult to observe. A new method incorporating the effects of noise was demonstrated, and it was applied to a group of PKiKP/PcP amplitude ratio measurements from highest quality recordings originated from a nuclear explosion at the Lop Nor test-site. First, a simple, explosive source radiation pattern was chosen

to alleviate problems associated with the uncertainty of source mechanisms. Second, the recordings at very short epicentral distances were considered with a goal of minimizing problems related to different sampling of PcP and PKiKP waves through the mantle. Eight new high-quality measurements are reported for individual stations.

The median values of the measured PKiKP/PcP amplitude ratios agree remarkably well with the theoretical values, oscillating around the ak135 (and similarly, PREM) value for the ICB density contrast. Depending on the epicentral distance, the six out of eight medians fall below the  $900 \text{ kg m}^{-3}$  mark, and the medians for the two measurements between  $16$  and  $18^\circ$  epicentral distance point to the density contrast as small as  $200\text{--}300 \text{ kg m}^{-3}$ . Such a small estimate of the density contrast from body waves could still produce the desired effect on the compressional velocity profile in the thermochemical boundary layer at the bottom of the outer core and return a modest heat flux from the inner core with a substantial inner core age, but only if accompanied by a small estimate of the density contrast of about  $400 \text{ kg m}^{-3}$  from normal modes (Gubbins *et al.* 2008). The CMB density ratio could be sporadically higher than average and this could also result in low PKiKP/PcP amplitude ratios. Furthermore, there are some indications that the ICB could be a rough boundary (e.g. Poupinet & Kennett 2004), or that the inner core just below the ICB could have a pattern of solidified and less solidified texture (e.g. Cormier 2007). If the ICB is characterized with such a mosaic of variable density contrast to which seismic body waves are sensitive, it is likely that the density fluctuations are restrained to the top of the inner core. Bergman (2003) argued that at least the top of the inner core is a dendritic mushy zone, in which interdendritic fluid pockets likely coexist to explain the observed nature of attenuation (e.g. Cormier *et al.* 1998) and attenuation in anisotropy of body waves (e.g. Creager 1992; Souriau & Romanowicz 1996; see Tkalčić & Kennett 2008 for a review). If PKiKP waves reflect from the inner core at the places where less dense features at the top of the inner core reduce the density contrast, than this could explain the observed lower values for stations VOS and ZRN. Some authors also argued that it is possible that at the base of the outer core there may exist a compositional change and/or a large-scale temperature difference and that inner core formation processes may be different between the two hemispheres (Yu *et al.* 2005), which would also require laterally varying density contrast at the ICB.

In a recent study, Krasnoshchekov *et al.* (2005) argued for a mosaic structure at the ICB, explaining it by lateral variations of ICB reflection coefficient due to changes in ICB fine structure and/or composition. While we conclude that the ICB could be laterally variable, we strongly disagree that shallow structures (upper mantle and crust) and or the inhomogeneities at the CMB's could not be sources of significant PcP and PKiKP amplitude fluctuations and high frequency content. For example, we previously explained the origin of a high frequency content of PKPPKP precursors by heterogeneous structure in lithosphere (Tkalčić *et al.* 2006), and we have recently demonstrated that the amplitudes of PKiKP and PcP could be negatively correlated as a result of a small-scale heterogeneity in the crust and upper mantle (Tkalčić *et al.* 2009). At this point in time, we favour strong variability in Earth structure as an explanation for fluctuations in the observed PKiKP/PcP amplitudes, although we here focus on how seismic noise can have a strong influence on amplitude measurements.

The uncertainties accompanying the median estimates including the noise effects are large (Table 1; Fig. 17). Although lower bounds of such defined uncertainties preclude estimates of the likely minimal ICB density contrast, the upper bounds of uncertainties now clearly point to the value of  $1100\text{--}1200 \text{ kg m}^{-3}$ . The comparison of the uncertainty bars with a range of theoretical ICB density ratio values, demonstrate quite clearly the limitations of methods that use the ray theory approximations. The uncertainties associated with the consideration of seismic noise might be at least partly an explanation for previous discrepancies in ICB density contrast estimates. The method used here is somewhat time-consuming and produces somewhat conservative, but very robust amplitude ratio uncertainties. Keeping all the assumptions and limitations in mind, it could be used for similar applications where it is necessary to measure amplitudes in time domain. With an increasing number of data, the method could be expanded to other robust observations of PcP and PKiKP waves on the same seismogram, normalizing measurement errors by event amplitudes. It remains to be seen if further improvements can be made and uncertainties in the ICB density contrast further reduced.

## ACKNOWLEDGMENT

We would like to thank P. G. Richards and an anonymous reviewer for useful suggestions on how to improve the manuscript. V. F. Cormier's participation was supported by a grant from the Vice Chancellor of the Australian National University funding travel as a Visiting Fellow, and by the National Science Foundation under grant EAR 07-38492.

## REFERENCES

- Aki, K. & Richards, P.G., 2002. *Quantitative Seismology: Theory and Methods*, 2nd edn, University Science Books, Sausalito, CA.
- Aubert, J., Amit, H., Hulot, G. & Olson, P., 2008. Thermochemical flows couple the Earth's inner core growth to mantle heterogeneity, *Nature*, **454**, 758–761.
- Bergman, M.I., 2003. Solidification of the Earth's core, in *Earth's Core: Dynamics, Structure, Rotation, Geodyn. Ser.*, pp. 105–127, eds Dehant, V. *et al.*, AGU, Washington, DC.
- Bolt, A.B. & Qamar, A., 1970. Upper bound to the density jump at the boundary of the Earth's inner core, *Nature*, **228**, 148–150.
- Buffett, B.A., Huppert, H.E., Lister, J.R. & Woods, A.W., 1996. On the thermal evolution of the Earth's core, *J. geophys. Res.*, **101**, 7989–8006.
- Cao, A. & Romanowicz, B., 2004. Constraints on Density and Shear Velocity Contrasts at the Inner Core Boundary, *Geophys. J. Int.*, **157**, 1–6.
- Červený, V., 2001. *Seismic Ray Theory*, Cambridge University Press, Cambridge.
- Cormier, V.F., 2007. Texture of the uppermost inner core from forward- and back-scattered seismic waves, *Earth planet. Sci. Lett.*, **258**, 442–453.
- Cormier, V.F., 2009. A glassy lowermost outer core, *Geophys. J. Int.*, in press.
- Cormier, V.F. & Richards, P.G., 1976. Comments on “The Damping of Core Waves” by Anthony Qamar and Alfredo Eisenberg, *J. geophys. Res.*, **81**, 3066–3068.

- Cormier, V.F., Xu, L. & Choy, G.L., 1998. Seismic attenuation of the inner core: viscoelastic or stratigraphic?, *Geophys. Res. Lett.*, **25**, 4019–4022.
- Creager, K.C., 1992. Anisotropy of the inner core from differential travel times of the phases PKP and PKIKP, *Nature*, **356**, 309–314.
- Doornbos, D.J. (ed.), 1988. *Seismological Algorithms*, Academic Press, London.
- Dziewonski, A.M. & Anderson, D.L., 1981. Preliminary reference Earth model, *Phys. Earth planet. Int.*, **25**, 297–356.
- Gubbins, D., Masters, G. & Nimmo, F., 2008. A thermochemical boundary layer at the base of Earth's outer core and independent estimate of core heat flux, *Geophys. J. Int.*, **174**, 1007–1018.
- Kennett, B.L.N., Engdahl, E.R. & Buland, R., 1995. Constraints on the velocity structure in the Earth from travel times, *Geophys. J. Int.*, **122**, 108–124.
- Koper, D.K. & Pyle, M.L., 2004. Observations of PKiKP/PcP amplitude ratios and implications for Earth structure at the boundaries of the liquid core, *J. geophys. Res.*, **109**, B03301, doi:10.1029/2003JB002750.
- Koper, K.D. & Dombrovskaya, M., 2005. Seismic properties of the inner core boundary from PKiKP/P amplitude ratios, *Earth planet. Sci. Lett.*, **137**, 680–694.
- Krasnoshechekov, D.N., Kaazik, P.B. & Ovtchinnikov, V.M., 2005. Seismological evidence for mosaic structure of the surface of the Earth's inner core, *Nature*, **435**, 483–487.
- Loper, D.E., 1983. Structure of the inner core boundary, *Geophys. Astrophys. Fluid Dyn.*, **25**, 139–155.
- Masters, T.G. & Gubbins, D., 2003. On the resolution of density within the Earth, *Phys. Earth planet. Int.*, **140**, 159–167.
- Nimmo, F., Price, G.D., Brodholt, J. & Gubbins, D., 2004. The influence of potassium on core and geodynamo evolution, *Geophys. J. Int.*, **156**, 363–376.
- Poupinet, G. & Kennett, B.L.N., 2004. On the observation of high frequency PKiKP and its coda in Australia, *Phys. Earth planet. Inter.*, **146**, 497–511.
- Richards, P.G., 1976. On the adequacy of plane-wave reflection/transmission coefficients in the analysis of seismic body waves, *Bull. seism. Soc. Am.*, **66**, 701–717.
- Shearer, P.M. & Masters, T.G., 1990. The density and shear velocity contrast at the inner core boundary, *Geophys. J. Int.*, **102**, 491–498.
- Song, X.D. & Helmberger, D.V., 1995. A P-wave velocity model of Earth's core, *J. geophys. Res.*, **100**, 9817–9830.
- Souriau, A. & Souriau, M., 1989. Ellipticity and density at the inner core boundary from subcritical PKiKP and PcP data, *Geophys. J. Int.*, **98**, 39–54.
- Souriau, A. & Romanowicz, B., 1996. Anisotropy in inner core attenuation: a new type of data to constrain the nature of the solid core, *Geophys. Res. Lett.*, **24**, 2103–2106.
- Stevenson, D.J., Spohn, T. & Schubert, G., 1983. Magnetism and thermal evolution of the terrestrial planets, *Icarus*, **54**, 466–489.
- Tkalčić, H. & Kennett, B.L.N., 2008. Core structure and heterogeneity: seismological perspective, *Aust. J. Earth Sci.*, **55**(4), 419–431. doi: 10.1080/08120090801888578.
- Tkalčić, H., Flanagan, M., & Cormier, V.F., 2006. Observations of near-podal P'P' precursors: evidence for back scattering from the 150–220 km zone in Earth's upper mantle. *Geophys. Res. Lett.*, **33**, L03305, doi:10.1029/2005GL024626.
- Tkalčić, H., Cormier, V.F. & Kennett, B.L.N., 2009. Steep reflections from the Earth's core reveal small-scale heterogeneity in the upper mantle, *Phys. Earth Planet. Int.*, submitted.
- Yu, W.-C., Wen, L. & Niu, F., 2005. Seismic velocity structure in the Earth's outer core, *J. geophys. Res.*, **110**, B02302, doi:10.1029/2003JB002928.
- Zou, Z., Koper, K.D. & Cormier, V.F., 2008. The structure of the base of the outer core inferred from seismic waves diffracted around the inner core, *J. geophys. Res.*, **113**, B05314, doi:10.1029/2007JB005316.